# Numerical Simulation of Ejected Molten Metal Nanoparticles Liquified by Laser Irradiation: Interplay of Geometry and Dewetting

S. Afkhami* and L. Kondic

*Department of Mathematical Sciences and Center for Applied Mathematics and Statistics, New Jersey Institute of Technology, Newark, New Jersey 07102, USA*

(Received 2 November 2012; published 16 July 2013)

Metallic nanoparticles, liquified by fast laser irradiation, go through a rapid change of shape attempting to minimize their surface energy. The resulting nanodrops may be ejected from the substrate when the mechanisms leading to dewetting are sufficiently strong, as in the experiments involving gold nanoparticles [Habenicht *et al.*, Science **309**, 2043 (2005)]. We use a direct continuum-level approach to accurately model the process of liquid nanodrop formation and the subsequent ejection from the substrate. Our computations show a significant role of inertial effects and an elaborate interplay of initial geometry and wetting properties: e.g., we can control the direction of ejection by prescribing appropriate initial shape and/or wetting properties. The basic insight regarding ejection itself can be reached by considering a simple effective model based on an energy balance. We validate our computations by comparing directly with the experiments specified above involving the length scales measured in hundreds of nanometers and with molecular dynamics simulations on much shorter scales measured in tens of atomic diameters, as by M. Fuentes-Cabrera *et al.* [Phys. Rev. E **83**, 041603 (2011)]. The quantitative agreement, in addition to illustrating how to control particle ejection, shows utility of continuum-based simulation in describing dynamics on nanoscale quantitatively, even in a complex setting as considered here.

DOI: 10.1103/PhysRevLett.111.034501 PACS numbers: 47.11.−j, 68.08.−p, 68.55.−a, 81.16.Rf

The evolution of fluid drops deposited on solid substrates has been the focus of a large research effort for decades. More recently, this effort has been particularly extensive on the nanoscale, due to the relevance of nanostructures in a variety of fields, ranging from DNA sequencing to plasmonics [1,2], nanogmagnetism [3], and liquid crystal displays and solar panel designs [4]. For example, the size and distribution of metallic particles strongly affects the coupling of surface plasmons to incident energy [1]. Controlling this coupling has the potential for large increases in the yield of solar cell devices.

In addition to physical experiments, modeling and simulations provide significant insight into the effects governing the evolution of drops and other liquid structures. Numerical simulation has an advantage of allowing us to switch off some of the involved physical phenomena and therefore isolate the dominant ones. On the nanoscale, however, it is not trivial to decide on an appropriate simulation technique. Molecular dynamics (MD) simulations, while very powerful and presumably as close to a real physical picture as it is to our knowledge of the underlying interaction laws, are still extremely computationally demanding. Therefore, one would like to resort to the continuum-based simulation. However, it is not immediately clear that this approach is appropriate on the nanoscale where the basic assumptions of continuum fluid mechanics are pushed to their limits. In addition, the continuum simulation of free surface time-dependent problems based on full three-dimensional Navier-Stokes (NS) formulation is still computationally demanding. For this reason, this type of simulation is rarely attempted in practice, and instead the researchers resort to asymptotic (long-wave) methods. Such an approach has been applied with success to problems involving the wetting and dewetting of drops and films; see Ref. [5] for reviews. This direction is, however, questionable due to the inherent assumptions, in particular, when contact angles are large and inertial effects are significant. One such class of problems involves liquid metals. These configurations may even lead to topological changes under liquefaction with metal particles detaching from the substrate [6]. In such cases, long-wave theory clearly cannot be applied.

In this work, we show that direct numerical solutions of NS equations lead to the results which are in quantitative agreement with (i) MD simulations of dewetting of 1–1.5 nm thick, liquid copper (Cu) disks of radius of 10–15 nm, and (ii) physical experiments involving ''jumping'' gold (Au) nanoparticles of typical in-plane length scale in the range of 100 nm. While the utility of continuum mechanics on nanoscale problems involving liquid metals was discussed previously (see, e.g., Ref. [7]), as far as the authors are aware, this is the first attempt to compare explicitly continuum NS simulations both to MD and to physical experiments in a dynamic setting. Furthermore, we utilize the simulations to illustrate the dominant effects and discuss, in particular, the conditions leading to ejection of fluid material from the substrate. We also present an effective model based on an energy balance to provide basic insight into the ejection mechanism. We first consider the dewetting of liquid Cu disks recently

 © 2013 American Physical Society

simulated by MD [8] and then shift focus to Au particles considered experimentally [6].

*Methods.*—The simulations are based on the volume of fluid (VOF) approach, which, when coupled to a flow solver, is also used to compute quantities related to surface tension that enter the flow calculation. Until recently, the VOF method was not deemed appropriate for the study of phenomena in which surface tension is the driving force. Recent improvements to calculating curvature and applying the surface tension force appear to resolve this issue [9]. Within this approach, one solves the three-dimensional NS equations that govern the motion of the fluid both inside the liquid domain and in the surrounding gas phase. For Cu disk structures, a free-slip boundary condition is specified at the substrate; this choice is motivated by the MD simulations [8]. This assumption is also consistent with the fact that the length scale associated with slip is nanometric for most systems [10]. When considering Au structures, the Navier slip [11] with a slip length of 3 nm is imposed; this particular value is obtained by direct comparison with the experiments [6] and is further discussed in the Supplemental Material [12]. Such a value is also consistent with the MD simulations [13], indicating slip lengths of a few nanometers for mesoscopic systems. The physical problem considered is the one of a Newtonian, isothermal, incompressible fluid, and therefore in the present work we do not consider the effects related to phase change and/or thermal variation of material properties occurring in experiments [6]. Simulations are carried out on an adaptive mesh [14], and numerical convergence has been verified by considering simulations with different grid resolutions [15]. See Ref. [12] for more details.

*Results.*—Figure 1(a) shows the evolution of a Cu disk of initial height $h_0 = 15$ Å and radius $R_0 = 150$ Å with an initial contact angle $\theta_0 = 90°$, when the equilibrium contact angle $\theta_{eq} = 80°$ that dewets and collapses into a spherical cap. Figures 1(b) and 1(c) show the front position $R(t)$ and velocity $\dot{R}(t)$, respectively. We also show the results of the MD simulations obtained by employing two different Lennard-Jones (LJ) potentials, LJ(a) and LJ(b), that differ by depth of potential well [8]. These results show that our numerical results and the MD simulations yield fully consistent retraction time scales. We also see that $\theta_{eq}$ influences the initial rapid retraction, with larger $\theta_{eq}$ leading to faster dynamics for early times.

A different type of evolution occurs if $\theta_{eq}$ is further increased. To illustrate this, Fig. 2(a) shows snapshots of

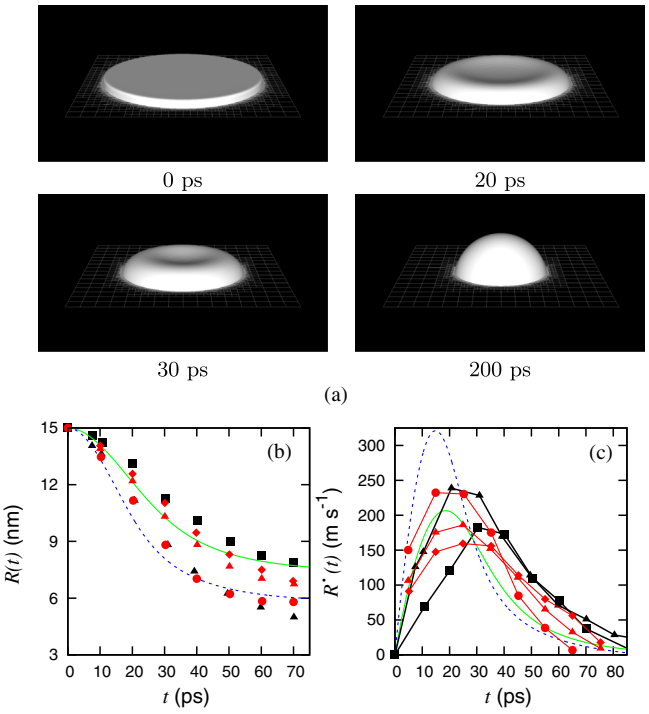


FIG. 1 (color online). Evolution of a Cu disk ($h_0 = 15$ Å, $R_0 = 150$ Å, $\theta_0 = 90°$). (a) Snapshots for $\theta_{eq} = 80°$; (b) $R(t)$ and (c) $\dot{R}(t)$ for (filled rectangle) $\theta_{eq} = 80°$ and (filled upward triangle) $\theta_{eq} = 115°$ (black symbols). MD simulations for (filled circle) LJ (a), $\theta_{eq} = 116°$, and (filled diamond) LJ(b), $\theta_{eq} = 75.6°$, with $h_0 = 10$ Å and (filled upward triangle) LJ(b) with $h_0 = 15$ Å [8] (red symbols). Predictions of the model, Eq. (1), for $\theta_{eq} = 80°$ (solid green line) and 115° (dashed blue line). Oh ≈ 0.35.

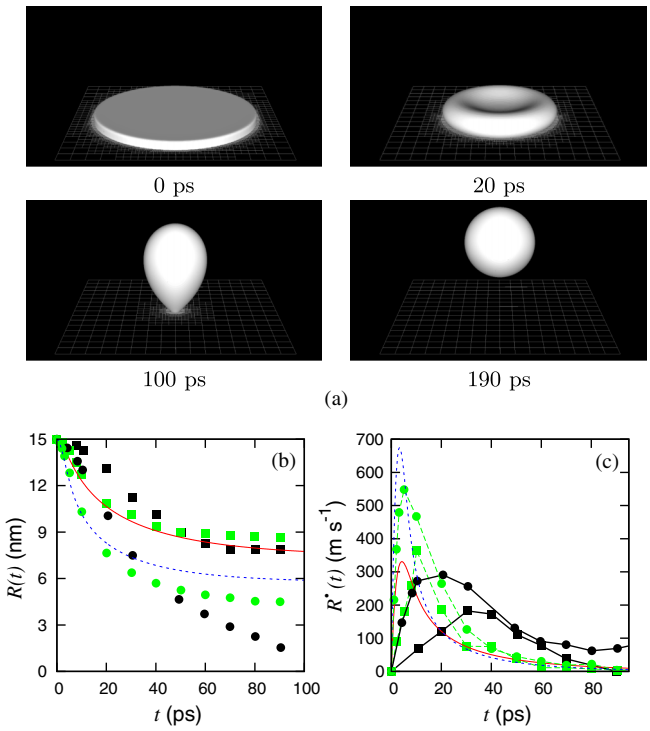


FIG. 2 (color online). Evolution of a disk ($h_0 = 15$ Å, $R_0 = 150$ Å, $\theta_0 = 90°$). (a) For $\theta_{eq} = 140°$, the disk detaches at around 100 ps (see also the animation in Ref. [12]); (b) $R(t)$ and (c) $\dot{R}(t)$ for $\theta_{eq} = 80°$ (filled rectangle) and 140° (filled circle) when Oh ≈ 0.35 (black symbols) and Oh ≈ 1.1 (green symbols). Predictions of the model, Eq. (1), for $\theta_{eq} = 80°$ (solid red line) and $\theta_{eq} = 140°$ (dashed blue line) when Oh ≈ 1.1.

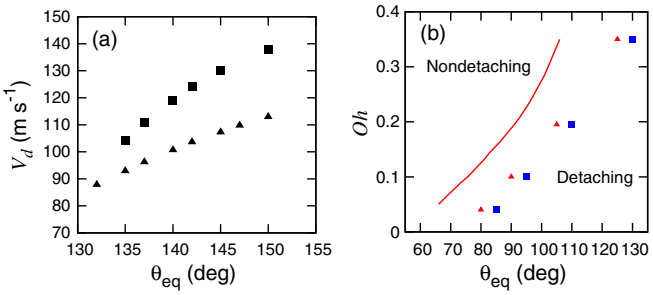


FIG. 3 (color online). (a) The effect of $\theta_{eq}$ on the ejection velocity $V_d$ for a Cu nanodisk ($h_0 = 15$ Å, $R_0 = 150$ Å) predicted by the model based on Eq. (1) (filled upward triangle) [see also Eq. (13) in Ref. [12]] and simulations (filled rectangle). (b) Phase diagram showing the influence of Oh and $\theta_{eq}$ on the ejection. The solid line is based on the model, Eq. (1) [see also Eq. (13) in Ref. [12]], and the symbols mark the result of the numerical simulation showing detaching (filled rectangle) and nondetaching (filled upward triangle) nanodrops. A linear fit to the solid line yields a slope of 0.0075.

the profiles for $h_0 = 15$ Å, $R_0 = 150$ Å, $\theta_0 = 90°$, and $\theta_{eq} = 140°$. For this $\theta_{eq}$, the contraction is so fast that the nanodrop jumps off the surface, following elongation in the $y$ direction (normal to the substrate). Similar behavior is observed for any $\theta_{eq} \gtrsim 130°$, again in quantitative agreement with the MD simulations [8].

To gain additional insight regarding the effects that drive contraction and possibly ejection of the fluid, we have carried out an additional set of simulations with modified inertial effects. This was implemented by varying incompressible fluid density, but more generally the dynamics can be characterized by the Ohnesorge number $\mathrm{Oh} = \eta/\sqrt{\rho\sigma R_0}$, which is related to the Reynolds number defined based on a characteristic capillary velocity $\sigma/\eta$ as $\mathrm{Re} = \mathrm{Oh}^{-2}$. For liquid Cu results in Fig. 1, $\mathrm{Oh} \approx 0.35$, suggesting that inertial effects are important; the same conclusion can be reached by considering an intrinsic length scale $\ell_v = \eta^2/(\rho\sigma)$, above which inertial effects become significant; for liquid Cu, $\ell_v \approx 1.78$ nm, therefore smaller than typical length scales considered here. As an example, Figs. 2(b) and 2(c) show $R(t)$ and $\dot{R}(t)$ for $\mathrm{Oh} \approx 0.35$ and $\mathrm{Oh} \approx 1.1$. Reduced inertial effects eliminate the most noticeable feature of the dewetting: nanodroplets do not detach from the surface for the same $\theta_{eq}$. Additional simulations have shown that even for $\theta_{eq} = 150°$, there is no detachment for $\mathrm{Oh} \approx 1.1$.

A basic understanding of the effects that drive the fluid evolution can be reached by a relatively simple effective model based on the balance of relevant energies. In this model, the evolution of the nanodisk obeys the energy balance equation

$$\frac{\partial}{\partial t}[E_k + E_s] + D = 0, \tag{1}$$

where $E_k$, $E_s$ are the kinetic and surface energy, respectively, and $D$ is the rate of energy loss due to viscous dissipation, neglecting the gravitational energy. In this model, we describe the nanodisk dynamics by a fluid cylinder evolving on a solid substrate; a similar model has been considered for a drop impact problem [16]. Here, $E_k = \rho \int_\Omega |\vec{V}|^2 d\Omega/2$, where the integration is over the fluid cylinder, and $\vec{V} = \vec{V}(\vec{x}, t)$ is the axially symmetric

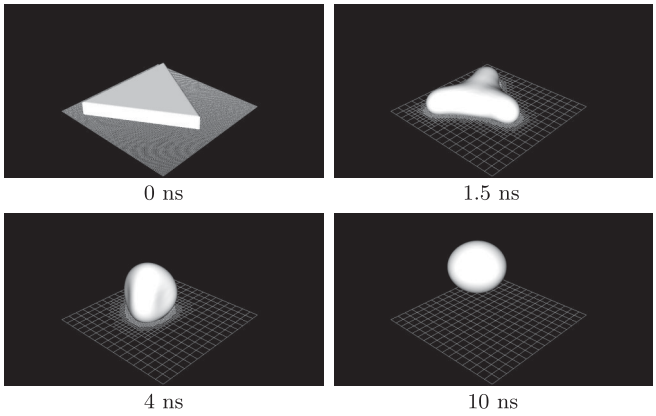


FIG. 4. Evolution of a Au equilateral triangle ($a = 405$ nm, $h_0 = 47$ nm, $\theta_0 = 90°$, and $\theta_{eq} = 140°$). The structure collapses into a droplet and detaches at $t \approx 7$ ns (see also the animation in Ref. [12]).

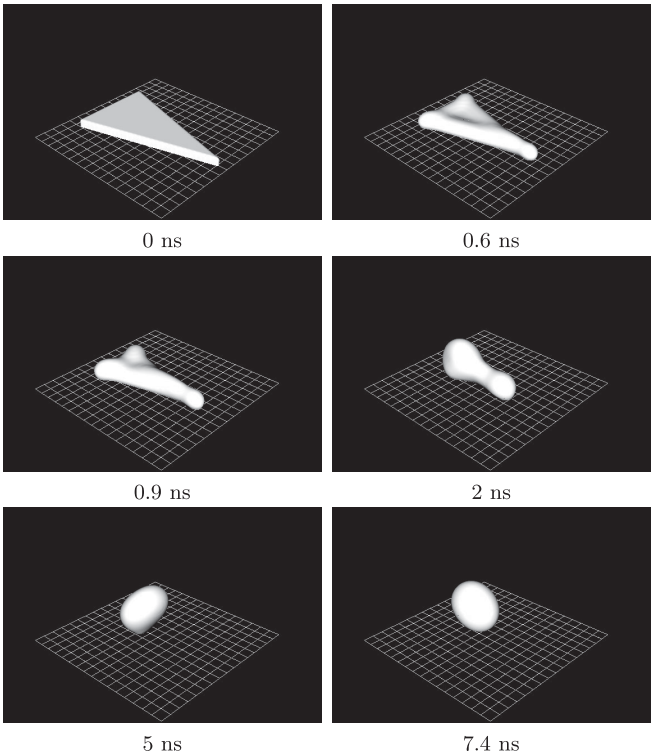


FIG. 5. Evolution of a Au isosceles triangle for $h_0 = 24$ nm, $\theta_0 = 90°$, long sides $a = 438$ nm and short side $b = 247$ nm; $\theta_{eq} = 140°$. The triangle collapses into a droplet and detaches from the substrate at around 5 ns (see also the animation in Ref. [12]).

fluid velocity. Using Young's law [17], $E_s = \sigma[\pi R(t)^2 \times (1 - \cos\theta_{eq}) + 2\pi R(t)h(t)]$, where $R(t)$ is the wetted radius and $h(t)$ is the cylinder height. The viscous dissipation energy $D = \int_\Omega (\tilde{\tau}: \vec{\nabla}\vec{V}) d\Omega$, where $\tilde{\tau}$ is the shear stress tensor. Using axisymmetric stagnation point flow and the conservation of mass, Eq. (1) reduces to a nonlinear second-order variable-coefficient ordinary differential equation given in Ref. [12]. This equation is then solved numerically, and the results are shown together with the computational results in Figs. 1 and 2 (plane lines). We find a very reasonable degree of agreement, suggesting that this simple model captures well the main mechanisms driving fluid contraction.

Figure 3 shows an additional comparison between the numerical simulation and the effective model. In Fig. 3(a), we observe that both the simulations and the model, Eq. (1), predict approximately linear dependence of the ejection velocity on $\cos\theta_{eq}$. We expect that the discrepancy between the two is mainly due to the deficiency of the model for large $\theta_{eq}$ [12]. Figure 3(b) shows a phase diagram in (Oh, $\theta_{eq}$) parameter space illustrating the criteria for ejection resulting from the model, together with the results of the numerical simulation, concentrating here on small values of Oh. Although the model underpredicts $\theta_{eq}$ required for ejection, we note a consistent trend of the results. Note that for large Oh $\approx 1.1$ considered previously, both the model and the simulation are in the nondetaching regime. Further investigation of the results of the model suggests that the ejection velocity increases approximately linearly as Oh decreases when $\theta_{eq}$ is fixed (see Ref. [12] for more details).

Next, we consider the configuration representative of physical experiments where Au triangular structures were liquified and let to evolve on a $SiO_2$ substrate [6]. Figure 4 shows the snapshots of an initially equilateral triangle ($\theta_0 = 90°$). The dewetting process first starts at the vertices, where the curvature is high. Because of high surface tension and large $\theta_{eq}$, the fluid starts to accumulate there. The humps at the vertices then coalesce into a droplet. Owing to a low viscosity of liquid gold, inertial effects dominate over viscous dissipation (here, Oh $\approx 0.047$ [12]), giving rise to an upward movement that leads to droplet detaching from the surface with a velocity of $\approx 24\ \mathrm{m\,s^{-1}}$. This process is consistent with the dewetting induced ejection mechanism outlined in Ref. [6]. We note the consistency of the time scales found by the simulations and the experiments in Ref. [6], where an ejection time scale of the order of 10 ns was observed. In addition to comparing favorably with experiments, the simulations allow for an additional insight since it is possible to explore very fast time scales and also easily vary the parameters, such as $\theta_{eq}$ and the initial shape, and ask what is their influence on the outcome.

To illustrate the influence of geometry, we consider isosceles triangles. Figure 5 shows a perhaps unexpected result, that despite the fact that the vertex at the smallest angle collapses the fastest due to a higher curvature, the vertices at the larger angles arrive sooner to the center (future work should analyze how general this result is). This mismatch excites oscillations of the droplet translating into a tumbling movement after the ejection.

Next, we ask whether the ejection angle $\alpha$ is always $\pi/2$. We find that $\alpha$ can be influenced for asymmetric collapse and present two means for controlling it by modifying (i) $\theta_{eq}$ and (ii) the initial geometry. Figures 6(a) and 6(b) show that increasing $\theta_{eq}$ alters the no ejection ($\alpha = 0$) to a directional ejection ($0 \le \alpha \le \pi/2$). A qualitative understanding can be reached by recalling that $\alpha \neq \pi/2$ is due to the lack of synchronicity of the collapse. A larger $\theta_{eq}$ results in higher surface energy, speeding up the fluid at the vertices. Therefore, for larger $\theta_{eq}$, collapse is more synchronous and $\alpha$ is closer to $\pi/2$. For smaller $\theta_{eq}$, $\alpha$ may vanish [see Figure 6(a)]; i.e., ejection does not happen, while an equilateral triangle with the same $\theta_{eq}$ does eject, illustrating the effect of asymmetry. We next consider the aspect ratio of the lengths ($a$, $b$) of triangle

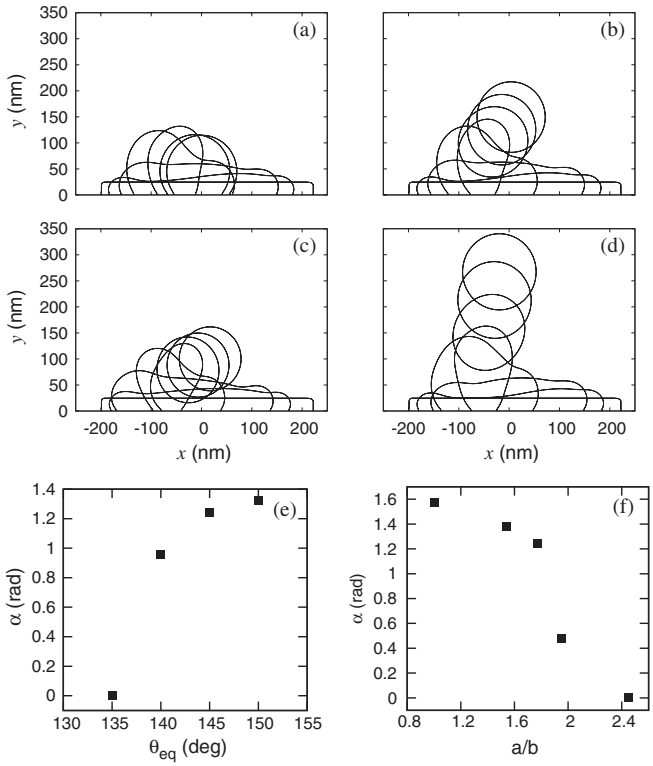


FIG. 6. $x$-$y$ cross sections of Au isosceles triangles for $h_0 = 24$ nm and $\theta_0 = 90°$. (a),(b) $a = 438$ nm and $b = 247$ nm for (a) $\theta_{eq} = 130°$, (b) 140°, showing the increase of ejection angle $\alpha$ as $\theta_{eq}$ is increased [note that in (a), $\alpha = 0$]; (c), (d) $\theta_{eq} = 145°$, and (c) $a = 362$ nm, $b = 185$ nm, (d) $a = 475$ nm, $b = 308$ nm; $t = 0$, 0.6, 1.2, 3, 4.4, 11, 19, 35 ns. (e),(f) Ejection angle $\alpha$ versus the $\theta_{eq}$ (e), when $a/b \approx 1.77$, and the initial geometrical ratio $a/b$ (f), when $\theta_{eq} = 145°$.

sides and find that the larger $a/b$ ratios lead to increased asymmetry of the collapse and smaller $\alpha$, as shown in Figs. 6(c) and 6(d).

Figures 6(e) and 6(f) show $\alpha$ versus $\theta_{eq}$ for fixed $a/b$ and versus $a/b$ for fixed $\theta_{eq}$, respectively. In Fig. 6(e), we see that the ejection angle increases monotonically with an increase of $\theta_{eq}$ with no ejection for $\theta_{eq} \lesssim 135°$. Figure 6(f) shows that $\alpha$ decreases with increased asymmetry and that for the considered $\theta_{eq}$, the ejection does not occur, i.e., $\alpha = 0$, when $a/b \gtrsim 2.4$. Very large ratios lead to a different type of dynamics: a Rayleigh-Plateau type of breakup; see Ref. [18] for discussion in the context of liquid metals. More elaborate analysis of the influence of geometry and wetting properties is needed to fully understand the dynamics—we leave this for future work.

*Conclusions.*—In this work, we have demonstrated that continuum simulations provide a good qualitative agreement with both MD simulations on the length scales in the range of 1–10 nm, and with the physical experiments with in-plane length scales measured in the range of 100 nm. We expect that this finding will further motivate modeling and computational work on these scales, since it is suggesting that the continuum-based simulation has a predictive power. For the problem of dewetting and possibly detaching nanodrops, the simulations provide precise insight regarding the influence of inertial, viscous, and capillary forces, in addition to the liquid-solid interaction. This insight is also confirmed by a simple model based on an energy balance and accounting for viscous energy losses. Furthermore, the simulations provide a clear prediction that the direction of the ejection of fluid from the substrate can be influenced (and controlled) by modifying either the wetting properties or the initial geometry. Future computational and modeling work will include the thermal and phase change effects, as well as more accurate modeling of liquid-solid interaction in the vicinity of contact lines, allowing us to even more accurately model the dynamics of liquid metals on the nanoscale.

*shahriar.afkhami@njit.edu

[1] S. Maier, *Plasmonics: Fundamentals and Applications* (Springer-Verlag, New York, 2007).
[2] H. Atwater and A. Polman, Nat. Mater. **9**, 205 (2010).
[3] S. Baderi, Rev. Mod. Phys. **78**, 1 (2006).
[4] S. A. Maier, P. G. Kik, H. A. Atwater, S. Meltzer, E. Harel, B. E. Koel, and A. A. G. Requicha, Nat. Mater. **2**, 229 (2003); S. Sun C. B. Murray, D. Weller, L. Folks, A. Moser, Science **287**, 1989 (2000).
[5] A. Oron, S. H. Davis, and S. G. Bankoff, Rev. Mod. Phys. **69**, 931 (1997); R. Craster and O. Matar, Rev. Mod. Phys. **81**, 1131 (2009).
[6] A. Habenicht, M. Olapinski, F. Burmeister, P. Leiderer, J. Boneberg, Science **309**, 2043 (2005).
[7] J. C. Burton, J. E. Rutledge, and P. Taborek, Phys. Rev. Lett. **92**, 244505 (2004).
[8] M. Fuentes-Cabrera, B. H. Rhodes, J. D. Fowlkes, A. López-Benzanilla, H. Terrones, M. L. Simpson, and P. D. Rack, Phys. Rev. E **83**, 041603 (2011).
[9] M. Sussman, J. Comput. Phys. **187**, 110 (2003); S. Afkhami and M. Bussmann, Int. J. Numer. Methods Fluids **57**, 453 (2008); **61**, 827 (2009).
[10] D. Bonn, J. Eggers, J. Indekeu, J. Meunier, and E. Rolley, Rev. Mod. Phys. **81**, 739 (2009).
[11] P. J. Haley and M. J. Miksis, J. Fluid Mech. **223**, 57 (1991).
[12] See Supplemental Material at http://link.aps.org/supplemental/10.1103/PhysRevLett.111.034501.
[13] T. Qian, X.-P. Wang, and P. Sheng, Phys. Rev. Lett. **93**, 094501 (2004).
[14] S. Popinet, J. Comput. Phys. **190**, 572 (2003).
[15] S. Afkhami, S. Zaleski, and M. Bussmann, J. Comput. Phys. **228**, 5370 (2009).
[16] H.-Y. Kim and J.-H. Chun, Phys. Fluids **13**, 643 (2001); P. Attané, F. Girard, and V. Morin, Phys. Fluids **19**, 012101 (2007).
[17] T. Young, Philos. Trans. R. Soc. London **95**, 65 (1805).
[18] L. Kondic, J. A. Diez, P. D. Rack, Y. Guan, and J. D. Fowlkes, Phys. Rev. E **79**, 026302 (2009); J. D. Fowlkes, L. Kondic, J. Diez, Y. Wu, and P. D. Rack, Nano Lett. **11**, 2478 (2011).